photonics

MDPI

Article

Study of the Interference Color with Nomarski Prism Wedge Angle in a Differential Interference Contrast Microscopy System

Fei Li and Tingyu Zhao *

Department of Physics, Key Laboratory of Optical Field Manipulation of Zhejiang Province, Zhejiang Sci-Tech University, 928 2nd Street, Hangzhou 310018, China
* Correspondence: zhaotingyu@zstu.edu.cn

Abstract: Differential interference contrast microscopy systems demonstrate the phase (optical path) rather than the amplitude of a sample. Previous studies have usually approximated the optical path difference produced by the Normarski prism. We derive the mathematical expression for the optical path difference produced by the incident light at any position of the Nomarski prism. As a result, the optical path difference introduced by the differential interference contrast microscope can be calculated. Moreover, the optical path difference is linearly related to the position of the incident light. In addition, the differential interference contrast microscopy system uses a composite light source, while previous studies were basically performed at a single wavelength. The standard wavelengths d (656 nm), F (587 nm), and C (486 nm) are taken as examples to analyze the relationship between the interference color change of the observation surface under the superposition of different wavelengths and the prism wedge angle when the prism moves. When the prism moves the same distance, the larger the prism wedge Angle is, the faster the interference color change is. The analysis based on practical considerations in this paper is believed to provide a method for studying Nomarski prisms.

Keywords: differential interference contrast; Nomarski prism; plane of apparent splitting; splitting angle

Citation: Li, F.; Zhao, T. Study of the Interference Color with Nomarski Prism Wedge Angle in a Differential Interference Contrast Microscopy System. *Photonics* **2023**, *10*, 678. https://doi.org/10.3390/photonics10060678

Received: 2 May 2023
Revised: 4 June 2023
Accepted: 8 June 2023
Published: 11 June 2023

1. Introduction

In recent years, reflective differential interference contrast (DIC) digital microscopy system has been widely used in precision processing and inspection fields, such as the observation of conductive particles in thin-film transistor liquid crystal displays [1], the measurement of martensite microstructures, and the classification of individual dielectric nanoparticles [2,3]. DIC microscopy system can be used for qualitative or quantitative measurements of samples [4–7], as well as for reflective surface assessment [8] and optical profiling [9].

As one of the main 3D morphological tools available for microsurface inspection, differential interference contrast microscopy [10] can transform small phase or optical path length variations on the object surface into light intensity, i.e., the phase or optical path length variations on the object surface are transformed into intensity variations due to the interference of light from two closely separated points on the object surface. It shows the subtle bumps on the sample surface with strong light intensity and interference color variations. The images captured by the DIC microscopy system have a distinctive shadow effect and a strong three-dimensional relief.

Studying the Nomarski prism is of utmost importance as it serves a critical function in differential interference contrast microscopy. Numerous researchers have conducted meticulous studies on the design theory of Nomarski prisms and engaged in DIC microscopy [11–20]. Early studies proposed simplified mathematical theoretical models for DIC imaging, such as the DIC imaging model constructed based on differential

methods [21,22]. These studies provided a good research basis and reference value for accurate models in later research. However, these imaging models did not take into account the phase difference produced by the light in the Nomarski prism itself, so they were only suitable for qualitative observation of the sample and could not be used for quantitative measurements.

In order to use the differential interference contrast microscopy for quantitative measurements, the phase change due to the Nomarski prism must be calculated. The above theoretical study only calculated the phase change for the half of the light path, i.e., the linearly polarized light incident to the prism and out to the intersection of the two linearly polarized beams, and did not take into account the light incident to the Nomarski prism, reflected from the sample surface and then returned to the Nomarski prism, and the outgoing process. Hartman [23] makes an approximation to the phase change caused by the Nomarski prism and does not obtain an exact solution. In this paper, the theoretical calculation of the phase difference arising during the passage of the incident light through the prism to the horizontal viewing plane and back to the prism is investigated based on the incident light perpendicular to the plane of apparent splitting, covering the entire light path and obtaining an algebraic solution.

In addition, previous theoretical studies of differential interference contrast microscopy systems have been dominated by single wavelength analysis. Practical differential interference contrast microscopy systems usually use a composite light source containing multiple wavelengths, such as white light, rather than a monochromatic source. The standard wavelengths d (656 nm), F (587 nm), and C (486 nm) are taken as examples to analyze the relationship between the interference color change of the observation surface under the superposition of different wavelengths and the prism wedge angle when the prism moves.

The research content of this paper includes three parts. In Section 2, we derive an expression between the prism parameters based on a geometric model of incident light perpendicular to the plane of apparent splitting and then derive the relationship between the optical path difference produced by the light in the prism as it is incident to the prism and reflected the prism through the image plane and the position of the incident light. In Section 3, we discuss the effect of different prism wedge angles on the interference color when the prism is moved at the same distance under a superposition of light intensities of multiple wavelengths. We briefly draw a conclusion in Section 4.

2. Methods

Figure 1 shows a diagram of the incidence plane of a Nomarski prism with a wedge angle of γ, the thickness of the prism d, δ the angle between the crystal axis of the first crystal and the lower surface (axially orthogonal), and the optical axis of the second crystal perpendicular to the incidence plane, which divides the optical system into zones 1, 2, 3 and 4. Assuming that the linearly polarized light is incident on the prism at an angle of incidence α, ε is the angle of separation between the ordinary(o) and extraordinary(e) rays, where the principal refractive index of the ordinary ray is n_o, and the principal refractive index of the extraordinary ray is n_e.

First, we discuss the component of light whose vibrational direction is perpendicular to the incident surface—ray o in zone 2 and ray e in zone 3, and we can then obtain the exit angle β_{oe}, and the subscript oe indicates that the component of polarized light changes from ray o (zone 2) to ray e (zone 3). We call it ray oe.

$$\beta_{oe} = \sin^{-1}\left[n_e \sin\left[\sin^{-1}\left\{\frac{n_o}{n_e}\sin\left[\sin^{-1}\left[\frac{\sin\alpha}{n_o}\right]+\gamma\right]\right\}-\gamma\right]\right] \quad (1)$$

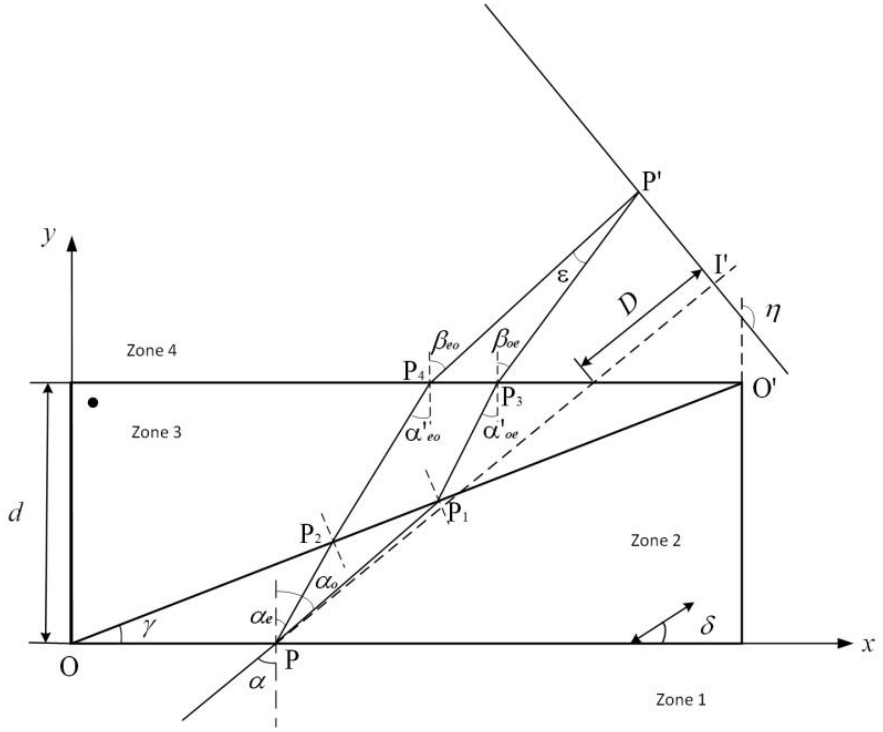

Figure 1. Optical schematic diagram of the Nomarski prism.

Then, we focus on the light component, whose vibrational direction is parallel to the incident surface, ray *e* in zone 2 and ray *o* in zone 3, and we can then obtain the exit angle β_{eo}, and the subscript *eo* indicates that the component of polarized light changes from ray *e* (zone 2) to ray *o* (zone 3). We call it ray *eo*.

$$\beta_{eo} = \sin^{-1}\left[n_o \sin\left[\sin^{-1}\left\{\frac{n_\theta}{n_o}\sin\left[\sin^{-1}\left[\frac{\sin\alpha}{n_\theta}\right]+\gamma\right]\right\}-\gamma\right]\right] \tag{2}$$

where, in Equation (2)

$$n_\theta = \frac{n_o n_e}{\left(n_o^2 \sin^2\theta + n_e^2 \cos^2\theta\right)^{1/2}} \tag{3}$$

where θ is the angle between the direction normal to the ray *e* light in zone 2 and the crystal optical axis.

The detailed derivation process of Equations (1) and (2) is shown in Appendix A.

Therefore, the beam splitting angle ε after the two beams exit through the prism is

$$\varepsilon = \beta_{oe} - \beta_{eo} \tag{4}$$

The right-angle coordinate system is shown in Figure 1, and η represents the angle between the ray intersection plane and the positive direction of the *y*-axis. Let the coordinates of the incident point be $\mathrm{P}(X_0, 0)$, the coordinates of rays *o* and *e* on the second dividing plane are $\mathrm{P}_1(X_o, Y_o)$ and $\mathrm{P}_2(X_e, Y_e)$, respectively; the coordinates of rays *oe* and *eo* on the third dividing plane are $\mathrm{P}_3(X_{oe}, Y_{oe})$ and $\mathrm{P}_4(X_{eo}, Y_{eo})$, respectively; the two beams intersect at the point $\mathrm{P}'(X_0', Y_0')$.

The geometric path of light in zone 2 is

$$t_o = \overline{\mathrm{PP}_1} = \frac{X_0 \sin\gamma}{\cos(\alpha_o + \gamma)} \tag{5}$$

where α_o is the refraction angle of ray o in zone 2; then, the coordinates of point P_1 as

$$\begin{aligned} X_o &= X_0 + t_o \sin\alpha_o \\ Y_o &= t_o \cos\alpha_o \end{aligned} \tag{6}$$

Similarly, the coordinates of point P_3 can be found as

$$\begin{aligned} X_{oe} &= X_0 + t_o \sin\alpha_o + (d - Y_o)\tan\alpha'_{oe} \\ Y_{oe} &= d \end{aligned} \tag{7}$$

where α'_{oe} is the angle of incidence at the junction of zone 3 and zone 4, and the geometric path of ray e in zone 2 is

$$t_e = \overline{PP_2} = \frac{X_0 \sin\gamma}{\cos(\alpha_e + \gamma)} \tag{8}$$

where α_e is the refraction angle of ray e in zone 2; then, the coordinates of point P_2 as

$$\begin{aligned} X_e &= X_0 + t_e \sin\alpha_e \\ Y_e &= t_e \cos\alpha_e \end{aligned} \tag{9}$$

Similarly, the coordinates of point P_4 can be found as

$$\begin{aligned} X_{eo} &= X_0 + t_e \sin\alpha_e + (d - Y_e)\tan\alpha'_{eo} \\ Y_{eo} &= d \end{aligned} \tag{10}$$

where α'_{eo} is the angle of incidence at the junction of zone 3 and zone 4, and the final two outgoing beams are determined by the following set of equations:

$$\begin{aligned} Y'_0 &= d + \frac{X'_0 - X_{oe}}{\tan\beta_{oe}} \\ Y'_0 &= d + \frac{X'_0 - X_{eo}}{\tan\beta_{eo}} \end{aligned} \tag{11}$$

Solving the coordinates of the intersection point of the two beams in Equation (11), we can obtain the following:

$$\begin{aligned} X'_0 &= \frac{X_{oe}\tan\beta_{eo} - X_{eo}\tan\beta_{oe}}{\tan\beta_{eo} - \tan\beta_{oe}} \\ Y'_0 &= d + \frac{X'_0 - X_{eo}}{\tan\beta_{eo}} \end{aligned} \tag{12}$$

The distance between the upper surface of the prism and the intersecting surface of the outgoing ray is $D = (Y'_0 - \frac{X'_0 - X_0}{\tan(90+\alpha)})\cos\alpha - \frac{d}{\cos\alpha}$.

The two polarized beams of light pass through the Nomarski prism and produce an optical path difference. The optical path of ray oe is

$$\begin{aligned} OPL_{oe} &= n_o\sqrt{(X_o - X_0)^2 + Y_o^2} + n_e\sqrt{(X_{oe} - X_o)^2 + (d - Y_o)^2} \\ &+ \sqrt{(X'_0 - X_{oe})^2 + (Y'_0 - d)^2} \end{aligned} \tag{13}$$

The optical path of ray eo is

$$\begin{aligned} OPL_{eo} &= n_\theta\sqrt{(X_e - X_0)^2 + Y_e^2} + n_o\sqrt{(X_{eo} - X_e)^2 + (d - Y_e)^2} \\ &+ \sqrt{(X'_0 - X_{eo})^2 + (Y'_0 - d)^2} \end{aligned} \tag{14}$$

Thus, the optical path difference between the two linearly polarized beams is

$$\Gamma = OPL_{oe} - OPL_{eo} \tag{15}$$

The phase difference is

$$\varphi = \frac{2\pi}{\lambda}\Gamma \tag{16}$$

In reflective differential interference contrast microscopy systems, as shown in Figure 2, light incident into the Nomarski prism gathers through the objective lens to the middle image plane, and then it reflects to the prism through the middle image plane and leaves the prism. The optical path difference mainly comes from the process of incidence and refraction of light in the prism.

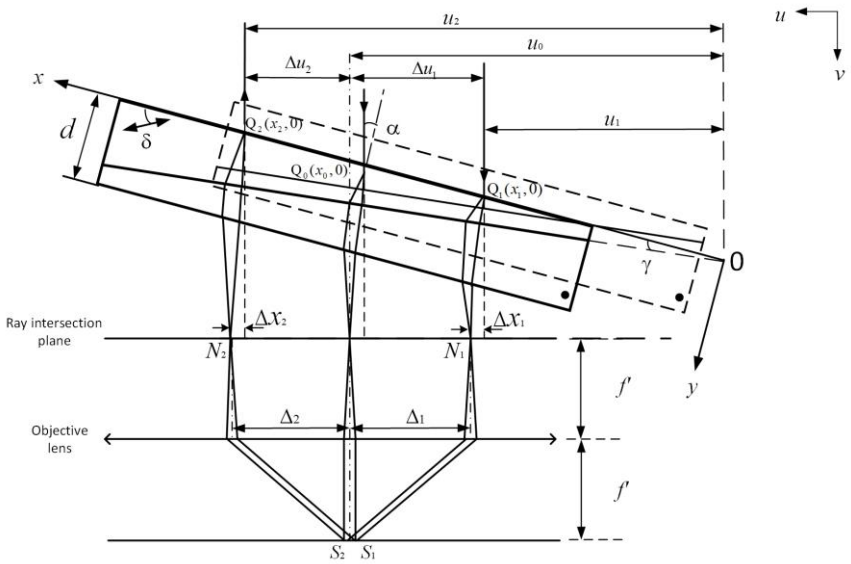

Figure 2. The schematic of the Nomarski prism, objective lens, and reflected light.

As shown in Figure 2, the light incident from point $Q_1(x_1, 0)$ into the Nomarski prism converges to the middle image plane through the objective lens and then reflects to the prism through the middle image plane and leaves the prism from point $Q_2(x_2, 0)$. In the whole process, Fermat's principle states that the actual path of a light ray between two points gives optical path length a stationary value. Since the family of rays from N_1 to N_2 are all actual paths, they all have the same optical path length. So, there is no optical path difference between the rays $N_1S_1N_2$ and $N_1S_2N_2$. The main optical path difference comes from two parts: the light incident into the prism, which refracted through the prism and reached the ray intersection plane, and the reflected light from the ray intersection plane to the prism, which emerges through the prism. Firstly, the optical path difference generated by the process of light incident from point $Q_1(x_1, 0)$ to the prism and reaching the ray intersection plane through prism refraction can be calculated using Equation (15). Because the optical path difference Γ caused by an incident on the Nomarski prism has a linear relationship with the incident coordinates x, when the incident coordinate x_1 is known, the coordinate x_2 of the reflected light on the prism can be calculated by geometric relation in Figure 2. We next calculate the optical path difference. When the prism moves horizontally along the ray intersection plane directly to the prism with the dotted line in Figure 2, the position of the incident light relative to the optical axis does not change because the optical axis of the system does not change, but the position relative to the prism surface changes, so the optical path difference also changes.

As shown in Figure 1, PI′ is the extension line of the incident light, and the incident point $P(X_0, 0)$ is set. The expression of the extension line of the incident ray can be obtained in the coordinate system based on a prism:

$$\begin{aligned} y_1 &= k_1 x + c_1 \\ k_1 &= \tan(90^\circ - \alpha) \\ c_1 &= -X_0 \tan(90^\circ - \alpha) \end{aligned} \tag{17}$$

where k_1 represents the slope and c_1 represents the intercept of the incident ray.

Because the plane of intersection of the ray of the Nomarski prism in the differential interference contrast microscope coincides with the rear focal plane of the objective lens, we need to make the incident ray extend perpendicular to the plane of intersection of ray:

$$\eta - \alpha = \frac{\pi}{2} \tag{18}$$

The ray direction satisfying the above formula is the optical axis direction of the differential interference contrast optical system so that we can find the linear expression of the plane of intersection of rays:

$$\begin{array}{l} y_2 = k_2 x + c_2 \\ k_2 = -\frac{1}{k_1} \\ c_2 = Y_0' - k_2 X_0' \end{array} \tag{19}$$

where k_2 is the slope of the line between P′ and I′, and c_2 is the value at which the line intersects the positive y-axis.

By connecting (17) and (19), the intersection coordinate $\mathrm{I}'(x_j, y_j)$ can be obtained as

$$\begin{array}{l} x_j = -\frac{c_1 - c_2}{k_1 - k_2} \\ y_j = k_1 x_j + c_1 \end{array} \tag{20}$$

From the coordinates of P′ and I′, the offset $\overline{\mathrm{P}'\mathrm{I}'}$, represented by Δx, can be obtained from the geometric relationship in Figure 2.

$$\Delta x = \overline{\mathrm{P}'\mathrm{I}'} = \frac{y_j - Y_0'}{\sin \alpha} \tag{21}$$

We take the wedge angle $\gamma = 0.4°$, the optical axis inclination angle $\delta = 100.5°$, and the prism thickness of the Nomarski prism as 2 mm; the optimized parameters are the light incidence angle $\alpha = -6.1032°$ and the plane distance between the upper surface of the prism and the ray D = 25.9643 mm. By substituting the above data into Equations (15) and (21), the offset Δx generated by different incident light positions passing through the prism can be obtained, as shown in Figure 3.

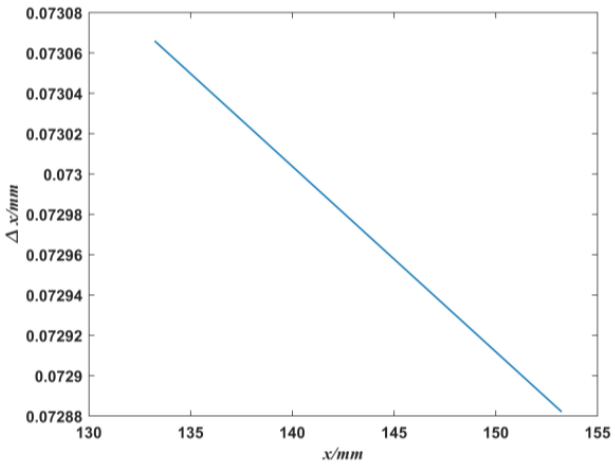

Figure 3. The relationship of the offset Δx and the ray incident position x.

As can be seen from Figure 3, Δx has a linear relationship with x. That is, the offset generated by each incident point through the prism (the difference between the incident ray extension line and its intersection point on the plane of intersection of ray) can be determined using Equation (21).

Figure 2 shows that, when the Nomarski prism is placed at an angle (for the purpose of parallel coincidence between the ray intersection plane and the objective lens), light incident into the prism passes through the objective lens to the viewing surface and then reflects from the viewing surface to the prism and out. In Figure 2, u_1 corresponds to the incident light, and u_2 corresponds to the light emitted through the prism after reflection, with the following relation expression:

$$\begin{aligned} x_0 &= \tfrac{u_0}{\cos\alpha} \\ x_1 &= \tfrac{u_1}{\cos\alpha} \\ x_2 &= \tfrac{u_2}{\cos\alpha} \end{aligned} \tag{22}$$

where x_0, x_1, and x_2 are the values in the x-y coordinate system; u_0, u_1, and u_2 are the values in the u-v coordinate system. According to the geometric relation in Figure 2

$$\begin{aligned} \Delta u_1 &= u_0 - u_1 = (x_0 - x_1)\cos\alpha \\ \Delta u_2 &= u_2 - u_0 = (x_2 - x_0)\cos\alpha \end{aligned} \tag{23}$$

Similarly

$$\begin{aligned} \Delta_1 &= \Delta u_1 + \Delta x_1 \\ \Delta_2 &= \Delta u_2 + \Delta x_2 \end{aligned} \tag{24}$$

Because $\Delta_2 = \Delta_1$, we have,

$$(x_0 - x_1)\cos\alpha + \Delta x_1 = (x_2 - x_0)\cos\alpha + \Delta x_2 \tag{25}$$

As can be seen from Equation (21), in the x-y coordinate system, each x value corresponds to a Δx, and the relationship between them is linear, so Δx_2 can be simplified into the following relation:

$$\Delta x_2 = kx_2 + c \tag{26}$$

From Equations (25) and (26), we can calculate the value of x in the x-y coordinate system when the ray returns.

$$x_2 = \frac{(x_0 - x_1)\cos\alpha + \Delta x_1 - c + x_0\cos\alpha}{\cos\alpha + k} \tag{27}$$

When x_1 and x_2 values are known, the corresponding optical path difference can be determined by substituting in the equation. Then, the optical path difference generated during the whole process of light incident into the Nomarski prism and exiting is

$$\Gamma_{sum} = \Gamma_{x_1} + \Gamma_{x_2} \tag{28}$$

The phase difference is

$$\chi = \frac{2\pi}{\lambda}\Gamma_{sum} \tag{29}$$

The function expression of the change in light intensity of the observed surface along with the phase is as follows [24].

$$\begin{aligned} I &= I_{\max}[\mathrm{Q} + \tfrac{1}{2}(1 - \mathrm{Q})(1 - \cos\chi)] \\ \mathrm{Q} &= \tfrac{I_{\min}}{I_{\max}} \end{aligned} \tag{30}$$

For an ideal optical system, we have $I_{\min} = 0$, $I_{\max} = 1$, $\mathrm{Q} = 0$. Therefore, Equation (30) can be further simplified as

$$I = [\frac{1}{2}(1 - \cos\chi)] \tag{31}$$

Similarly, we take the Nomarski prism with wedge angle $\gamma = 0.4°$, optical axis inclination $\delta = 100.5°$, and prism thickness of 2 mm, and from Equation (28), we can obtain the relationship between the optical path difference Γ_{sum} generated during the whole process of light incident to the Nomarski prism and outgoing and the light incident coordinate x, as shown in Figure 4. Γ_{sum} is linearly related to x.

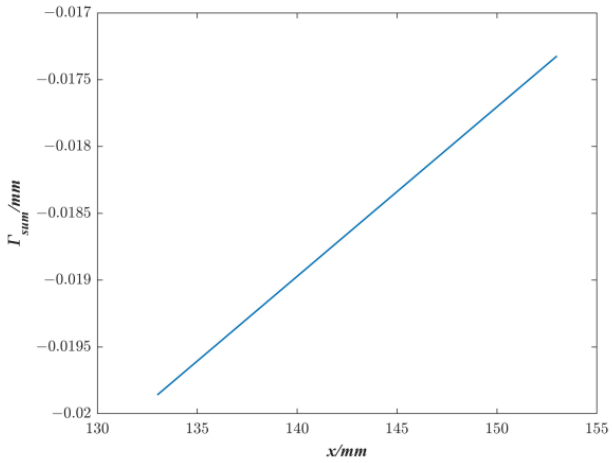

Figure 4. The relationship of optical path difference Γ_{sum} and the ray incident position x.

3. Simulation Results and Analysis

In the use of differential interference contrast (DIC) microscopy systems, it is necessary to adjust the position of the Normaski prism in the direction perpendicular to the optical axis to introduce a suitable optical path difference to obtain the best sample image. We found that the adjustment of the prism position brings about a change in the interference color. A specific analysis is presented below.

Assume that the prism length is 20 mm, and the thickness is d. As shown in Figure 5, the point where the intersecting prisms meet is considered the origin of coordinates in the absolute coordinate system. Half of the thickness is used as the center of the prism. If the prism wedge angle is γ_1, then the prism center transverse coordinate is x_1, and the prism is located at $[x_1 - 10, x_1 + 10]$, as shown in the gray area in Figure 5; if the prism wedge angle is γ_2, then the prism center transverse coordinate is x_2, and the prism is located at $[x_2 - 10, x_2 + 10]$, as shown in the green area in Figure 5 With the prism center as the initial position, it moves no further than the length of the prism itself, i.e., [−10 mm, 10 mm]. Therefore, we now use relative coordinates instead of absolute coordinates. Let the prism center be the zero point in relative coordinates, then its moving range is [−10 mm, 10 mm], as shown in Figure 6.

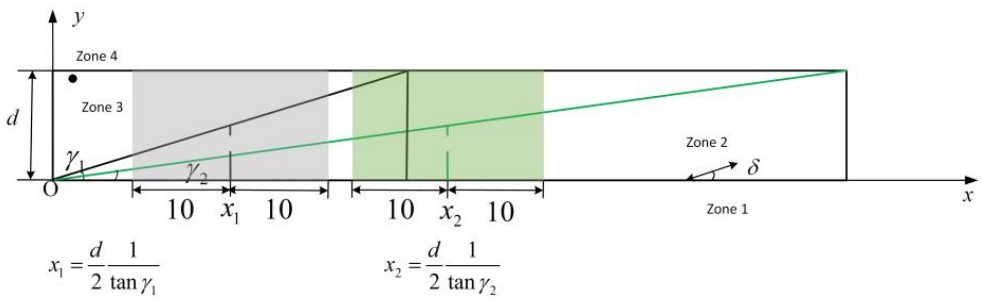

Figure 5. Schematic of the Nomarski prism.

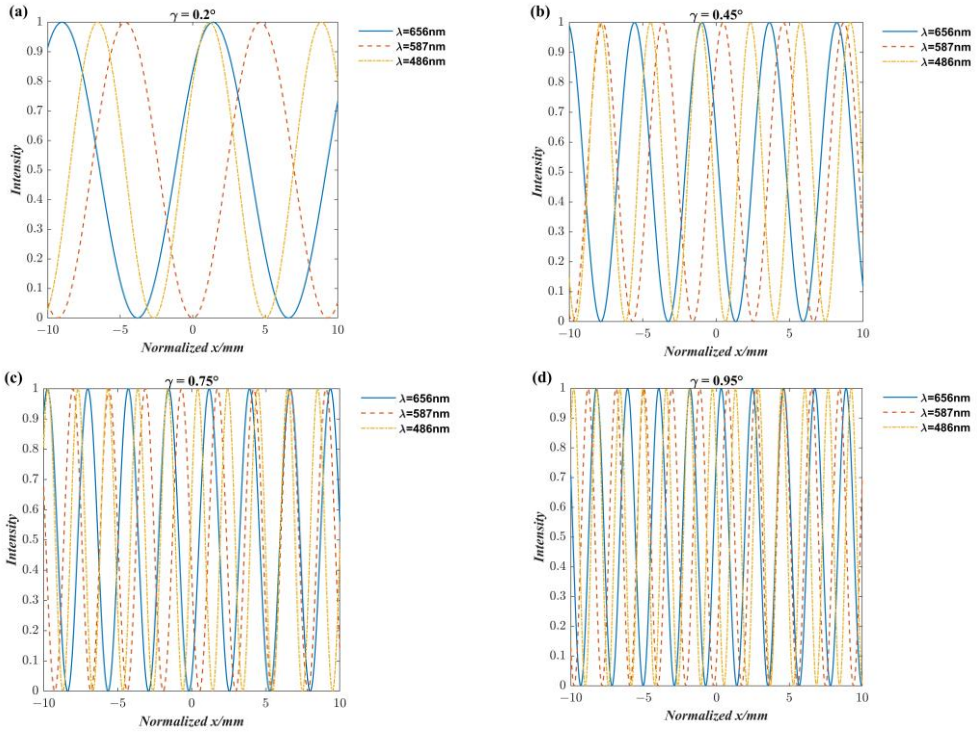

Figure 6. The relation diagram of prism position and light intensity at different wavelengths: (**a**) $\gamma = 0.2°$, (**b**) $\gamma = 0.45°$, (**c**) $\gamma = 0.75°$, and (**d**) $\gamma = 0.95°$.

Based on the above theory, three wavelengths of red light ($\lambda = 656$ nm), yellow-orange light ($\lambda = 587$ nm), and blue light ($\lambda = 486$ nm) in white light were selected. At the same time, the angle of the optical axis in the Nomarski prism was $\delta = 100.5°$, the thickness of the prism was 2 mm, and the wedge angle γ was 0.2°, 0.45°, 0.75°, and 0.95°, respectively. As shown in Figure 6, the horizontal coordinates indicate the position of the prism in the *x*-*y* coordinate system shown in Figure 2, and the difference between different coordinate values indicates the prism moves to the distance, and the vertical coordinates indicate the light intensity, where it can be seen from the comparison of (a), (b), (c) and (d) that the light intensity changes for more periods when the prism wedge angle is larger, and the prism moves the same distance.

As shown in Figure 7a, when the wedge angle $\gamma = 0.2°$, the prism moves from left to right, i.e., from -10 mm to 10 mm, and the interference color changes in the order of "red-cyan-green-black-rose-green-blue-violet." As shown in Figure 7b–d, the interference color changes faster as the wedge angle becomes larger when the prisms move the same distance. Taking the change from red to rose red as an example when the wedge angle γ is 0.2°, 0.45°, 0.75°, and 0.95°, the required moving distance is about 4.8 mm, 2.2 mm, 1.4 mm, and 1 mm, respectively. The larger the wedge angle, the shorter the moving distance required to change the same color. In other words, the larger the wedge angle is, the faster the interference color changes, provided that the same distance is moved. The results suggest that the prism wedge angle should be made as small as possible in the actual design of Nomarski. Otherwise, when the prism moves a tiny distance, it will produce multiple color changes in the observation screen, and it is not easy to find the best prism position for imaging.

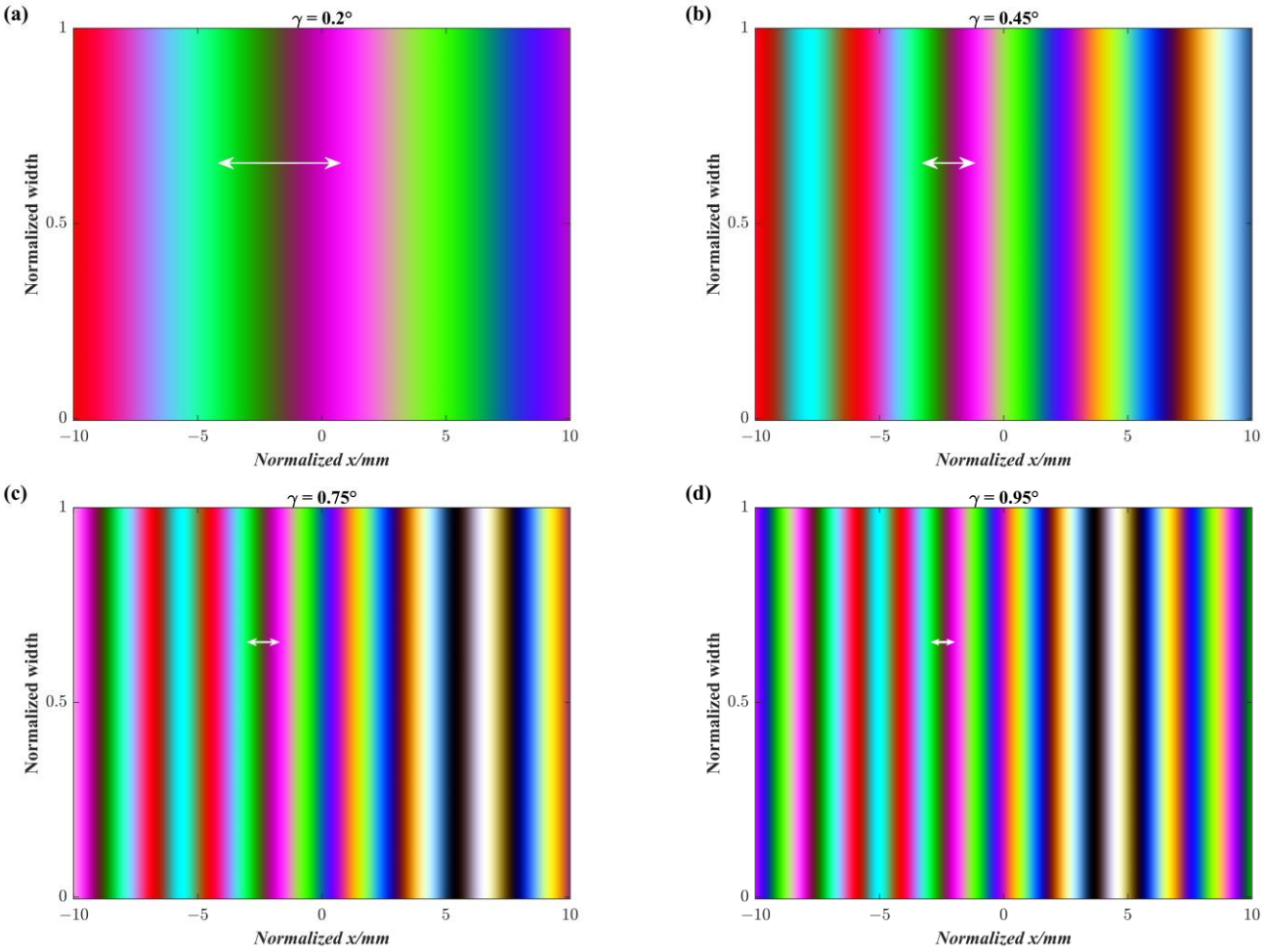

Figure 7. Schematic diagram of phase change light intensity superposition generated by prism movement: (**a**) $\gamma = 0.2°$, (**b**) $\gamma = 0.45°$, (**c**) $\gamma = 0.75°$, and (**d**) $\gamma = 0.95°$.

4. Conclusions

In differential interference contrast microscopy, the design of the Nomarski prism is a crucial technique. In practical application, it is not only necessary to make the incident light perpendicular to the plane of intersection of the light rays outside the prism but also to make the plane of intersection of the light rays coincide with the rear focal plane of the objective lens. Based on this principle, this paper deduces the optical path difference generated when the light incident on the prism is reflected from the observing surface and then comes out of the prism, and also discusses the relationship between the variation in the light intensity of the observing surface and the wedge angle of the prism when the prism moves at multiple wavelengths. The results suggest that the prism wedge angle should be made as small as possible in the actual design of Nomarski. Otherwise, when the prism moves a tiny distance, it will produce multiple color changes in the observation screen, and finding the best prism position for imaging is challenging.

Author Contributions: Conceptualization, T.Z. and F.L.; methodology, F.L.; software, F.L.; validation, F.L., and T.Z.; formal analysis, F.L.; investigation, F.L.; resources, T.Z.; data curation, F.L.; writing—original draft preparation, F.L.; writing—review and editing, F.L. and T.Z.; visualization, F.L.; supervision, T.Z.; project administration, F.L. All authors have read and agreed to the published version of the manuscript.

Funding: This research received no external funding.

Institutional Review Board Statement: Not applicable.

Informed Consent Statement: Not applicable.

Data Availability Statement: Data underlying the results presented in this paper are not publicly available at this time but may be obtained from the authors upon reasonable request.

Conflicts of Interest: The authors declare no conflict of interest.

Appendix A

When a beam of light is incident on a prism, it is divided into two beams, called *o* light and *e* light, due to the anisotropy of the light in the prism. As shown in Figure 1, linearly polarized light whose vibration direction is perpendicular to the paper surface is first discussed. This component is *o* light in zone 2 and has a refractive index of is n_o, which can be known from the refraction law when it passes through zone 1 and zone 2:

$$\begin{aligned} n_1 \sin\alpha &= n_{\mathrm{o}} \sin\alpha_{\mathrm{o}} \\ \alpha_{\mathrm{o}} &= \sin^{-1}\left(\tfrac{n_1}{n_{\mathrm{o}}}\sin\alpha\right) \end{aligned} \tag{A1}$$

where n_1 is the refractive index of linearly polarized light in zones 1 and 4, and since it is in air, its value is 1.

As shown in Figure 1, there is a geometric relation in $\Delta \mathrm{OPP}_1$

$$\alpha'_{\mathrm{o}} = \alpha_{\mathrm{o}} + \gamma \tag{A2}$$

In zone 3, the crystal optical axis is perpendicular to the paper surface, and the linearly polarized light component perpendicular to the paper surface is parallel to the crystal optical axis, which changes from o light to *e* light. Normally *e* light does not follow the law of refraction, so the law of refraction cannot be used. However, when the light propagation direction of *e* light is perpendicular to the direction of the crystal's optical axis, it follows the law of refraction. The direction of vibration of the *e* light in zone 3 is perpendicular to the direction of the crystal's optical axis, and the direction of the wave normal and the direction of the light coincide, so the line of polarized light follows the law of refraction, and the index of refraction at this time is n_e. Then, there is the following relationship between the interface zone 2 and zone 3:

$$\begin{aligned} n_o \sin\alpha'_o &= n_e \sin\alpha_{oe} \\ \alpha_{oe} &= \sin^{-1}\left(\tfrac{n_o}{n_e}\sin\alpha'_o\right) \end{aligned} \tag{A3}$$

In $\Delta \mathrm{P_1P_3O'}$ by the geometric relation, there is

$$\alpha'_{oe} = \alpha_{oe} - \gamma \tag{A4}$$

The refraction law is used at the interface between zone 3 and zone 4 and can be obtained from Equations (A1)–(A4)

$$\begin{aligned} n_1 \sin\beta_{oe} &= n_e \sin\alpha'_{oe} \\ \beta_{oe} &= \sin^{-1}\left[n_e \sin\left[\sin^{-1}\left\{\tfrac{n_o}{n_e}\sin\left[\sin^{-1}\left[\tfrac{\sin\alpha}{n_o}\right]+\gamma\right]\right\}-\gamma\right]\right] \end{aligned} \tag{A5}$$

For linearly polarized light whose direction of vibration is parallel to the surface of the paper. In zone 2 of Figure 1, the vibration direction of this component is in the same plane as the optical axis, so it is ray *e* at this time. The ray *e* propagates at an angle to the optical axis of the crystal. In this case, the direction of the wave normally will be separated from the light. Let the angle between the wave normal and the incident light normal be α_k. Therefore, the relationship between the direction of the light, the direction of the optical axis, and the direction of the wave normal is shown in Figure A1. The angle between the wave normal and the optical axis is θ.

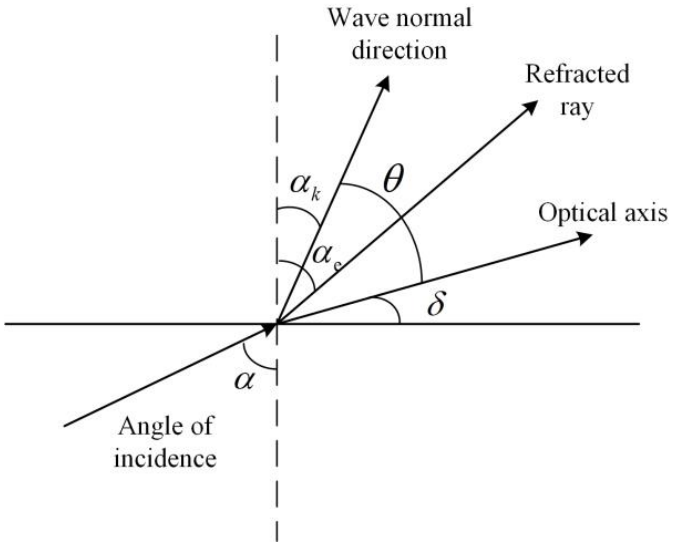

Figure A1. The relationship between the optical axis, wave normal, and the direction of light rays.

Because the direction of the wave normal obeys the law of refraction, the wave normal is used to derive the angle of *e*-light emission. The partition interface between zone 1 and zone 2 has

$$\begin{aligned} n_1 \sin\alpha &= n_\theta \sin\alpha_k \\ \alpha_k &= \sin^{-1}\left(\tfrac{n_1}{n_\theta}\sin\alpha\right) \end{aligned} \tag{A6}$$

where $n_\theta = \frac{n_o n_e}{(n_o^2 \sin^2\theta + n_e^2 \cos^2\theta)^{1/2}}$, according to the geometric relation in Figure A1, it can be obtained.

According to Figure 1, in the OPP by the geometric relationship, there is

$$\alpha_k' = \alpha_k + \gamma \tag{A7}$$

Since the vibration direction of the linearly polarized light perpendicular to the paper surface is the same as the direction of the optical axis in zone 3, the polarized light component changes from *e* light in zone 2 to *o* light in zone 3 at this time. It follows the law of refraction and has the following relationship at the interface between zone 2 and zone 3:

$$\begin{aligned} n_\theta \sin\alpha_k' &= n_\mathrm{o} \sin\alpha_{ko}, \\ \alpha_{ko} &= \sin^{-1}\left(\tfrac{n_\theta}{n_\mathrm{o}}\sin\alpha_k'\right). \end{aligned} \tag{A8}$$

Using the law of refraction at the partition between zones 3 and 4,

$$n_1 \sin\beta_{ko} = n_e \sin\alpha_{ko}' \tag{A9}$$

where α_{ko}' is obtained from the geometric relationship of $\Delta P_2P_4O\prime$ in Figure 1.

The direction of the wave normal in zone 3 is the same as the direction of the light, and the angle of emergence when the light leaves the interface between zone 3 and zone 4 can be obtained from Equations (A6)–(A9).

$$\beta_\mathrm{eo} = \beta_\mathrm{ko} = \sin^{-1}\left[n_o \sin\left[\sin^{-1}\left\{\frac{n_\theta}{n_o}\sin\left[\sin^{-1}\left[\frac{\sin\alpha}{n_\theta}\right]+\gamma\right]\right\}-\gamma\right]\right] \tag{A10}$$

References

1. Ni, G.; Liu, L.; Du, X.; Zhang, J.; Liu, J.; Liu, Y. Accurate AOI inspection of resistance in LCD Anisotropic Conductive Film bonding using differential interference contrast. *Optik* **2017**, *130*, 786–796. [CrossRef]
2. Zeng, Z.; Zhang, C.; Du, S.; Chen, X. Quantitative surface topography of martensitic microstructure by differential interference contrast microscopy. *J. Mech. Phys. Solids* **2018**, *124*, 102–114. [CrossRef]
3. Hamilton, S.; Regan, D.; Payne, L.; Langbein, W.; Borri, P. Sizing individual dielectric nanoparticles with quantitative differential interference contrast microscopy. *Analyst* **2022**, *147*, 1567–1580. [CrossRef] [PubMed]
4. Pluta, M. Nomarski's DIC microscopy: A review. *SPIE* **1994**, *1846*, 10–25. [CrossRef]
5. Hartman, J.S.; Gordon, R.L.; Lessor, D.L. Nomarski differential interference contrast microscopy for surface slope measurements: An examination of techniques. *Appl. Opt.* **1981**, *20*, 2665–2669. [CrossRef]
6. Lessor, D.L.; Hartman, J.S.; Gordon, R.L. Quantitative surface topography determination by Nomarski reflection microscopy I Theory. *J. Opt. Soc. Am.* **1979**, *69*, 357–366. [CrossRef]
7. Wei, Q.; Li, Y.; Vargas, J.; Wang, J.; Gong, Q.; Kong, Y.; Jiang, Z.; Xue, L.; Liu, C.; Liu, F.; et al. Principal component analysis-based quantitative differential interference contrast microscopy. *Opt. Lett.* **2018**, *44*, 45–48. [CrossRef]
8. Sochacka, M.; Staronski, L.R. Phase-stepping DIC technique for reflecting surface evaluation. Phase Contrast and Differential Interference Contrast Imaging Techniques and Applications. *SPIE* **1994**, *1846*, 222–233. [CrossRef]
9. Li, Q.; Gao, H.; Xue, S.; Li, Y. Optical profilometer based on the principle of differential interference. *Opt. Eng.* **2001**, *40*, 833–836. [CrossRef]
10. Allen, R.D.; David, G.B.; Nomarski, G. The zeiss-Nomarski differential interference equipment for transmitted-light microscopy. *Z Wiss. Mikrosk.* **1969**, *69*, 193–221. [PubMed]
11. Kagalwala, F.; Kanade, T. Simulating DIC microscope images: From physical principles to a computational model. In Proceedings of the Workshop on Photometric Modeling for Computer Vision and Graphics (Cat. No.PR00271), Fort Collins, CO, USA, 22 June 1999; pp. 48–55. [CrossRef]
12. Cogswell, C.J.; Smith, N.I.; Larkin, K.G.; Hariharan, P. Quantitative DIC microscopy using a geometric phase shifter. *Bio-Med. Opt.* **1997**, *2984*, 72–81. [CrossRef]
13. Arnison, M.R.; Larkin, K.G.; Sheppard, C.J.R.; Smith, N.I.; Cogswell, C.J. Linear phase imaging using differential interference contrast microscopy. *J. Microsc.* **2004**, *214*, 7–12. [CrossRef]
14. Kou, S.S.; Sheppard, C.J.R. Quantitative phase restoration in differential interference contrast (DIC) microscopy. *Opt. Digit. Image Process. SPIE* **2008**, *7000*, 46–53. [CrossRef]
15. Preza, C.; Snyder, D.L.; Rosenberger, F.U.; Markham, J.; Conchello, J.-A. Phase estimation from transmitted-light DIC images using rotational diversity. *SPIE—Int. Soc. Opt. Eng.* **1997**, *3170*, 97–107. [CrossRef]
16. Kagalwala, F.; Kanade, T. Reconstructing specimens using DIC microscope images. *IEEE Trans. Syst. Man Cybern. Part B* **2003**, *33*, 728–737. [CrossRef]
17. King, S.V.; Cogswell, C.J. A phase-shifting DIC technique for measuring 3D phase objects: Experimental verification. Three-Dimensional and Multidimensional Microscopy: Image Acquisition and Processing XI. *SPIE* **2004**, *5324*, 191–196. [CrossRef]
18. Ishiwata, H.; Itoh, M.; Yatagai, T. A new method of three-dimensional measurement by differential interference contrast microscope. *Opt. Commun.* **2006**, *260*, 117–126. [CrossRef]
19. Cui, X.; Lew, M.; Yang, C. Quantitative differential interference contrast microscopy based on structured-aperture interference. *Appl. Phys. Lett.* **2008**, *93*, 091113. [CrossRef]
20. Fu, D.; Oh, S.; Choi, W.; Yamauchi, T.; Dorn, A.; Yaqoob, Z.; Dasari, R.R.; Feld, M.S. Quantitative DIC microscopy using an off-axis self-interference approach. *Opt. Lett.* **2010**, *35*, 2370–2372. [CrossRef] [PubMed]
21. Holmes, T.J.; Levy, W.J. Signal-processing characteristics of differential-interference-contrast microscopy. *Appl. Opt.* **1987**, *26*, 3929–3939. [CrossRef] [PubMed]
22. Cogswell, C.J.; Sheppard, C.J.R. Confocal differential interference contrast (DIC) microscopy: Including a theoretical analysis of conventional and confocal DIC imaging. *J. Microsc.* **1992**, *165*, 81–101. [CrossRef]
23. Hartman, J.S.; Gordon, R.L.; Lessor, D.L. Development Of Nomarski Microscopy For Quantitative Determination Of Surface Topography (A). *Interferom. SPIE* **1979**, *192*, 223–230. [CrossRef]
24. Hartman, J.S.; Gordon, R.L.; Lessor, D.L. Quantitative surface topography determination by Nomarski reflection microscopy 2: Microscope modification, calibration, and planar sample experiments. *Appl. Opt.* **1980**, *19*, 2998–3009. [CrossRef] [PubMed]